# High-Throughput Characterization of Surface Segregation in CuxPd1−x Alloys

6 **AUTHORS**, INCLUDING:

Deepika Priyadarshini
IBM
**14** PUBLICATIONS **52** CITATIONS

SEE PROFILE

Yoosuf Picard
Carnegie Mellon University
**90** PUBLICATIONS **583** CITATIONS

SEE PROFILE

Andrew J. Gellman
Carnegie Mellon University
**278** PUBLICATIONS **5,113** CITATIONS

SEE PROFILE

# High-Throughput Characterization of Surface Segregation in $Cu_xPd_{1-x}$ Alloys

Deepika Priyadarshini,[†,‡] Petro Kondratyuk,[†,‡] Yoosuf N. Picard,[§] Bryan D. Morreale,[†] Andrew J. Gellman,[†,‡] and James B. Miller*,[†,‡]

[†]National Energy Technology Laboratory, U.S. Department of Energy, Pittsburgh, Pennsylvania 15236, United States

[‡]Department of Chemical Engineering and [§]Department of Materials Science and Engineering, Carnegie Mellon University, Pittsburgh, Pennsylvania 15213, United States

**ABSTRACT:** A high throughput methodology for the study of surface segregation in alloys has been developed and applied to the $Cu_xPd_{1-x}$ system. A novel offset-filament deposition tool was used to prepare $Cu_xPd_{1-x}$ composition spread alloy films (CSAFs), high throughput sample libraries with continuous lateral composition variation spanning the range $x = 0.05-0.95$. Spatially resolved low energy ion scattering spectroscopy (LEISS) and X-ray photoelectron spectroscopy (XPS) were used to characterize the films' top-surface and near-surface compositions, respectively, as functions of alloy composition, $x$, and temperature. Electron backscatter diffraction (EBSD) was used to identify the bulk phases in the CSAF as a function of alloy composition, $x$. Films equilibrated by annealing at temperatures $\geq$ 700 K displayed preferential segregation of Cu to their top-surfaces at all bulk compositions; segregation patterns did not, however, depend on local structure. The Langmuir—McLean thermodynamic model was applied to segregation measurements made in the temperature range 700—900 K in order to estimate the enthalpy ($\Delta H_{seg}$) and entropy ($\Delta S_{seg}$) of segregation as a function of bulk $Cu_xPd_{1-x}$ composition. Segregation measurements at $x = 0.30$ on the CSAF compare well with results previously reported for a bulk, polycrystalline $Cu_{0.30}Pd_{0.70}$ alloy, demonstrating the utility of the CSAF as a high throughput library for study of segregation.
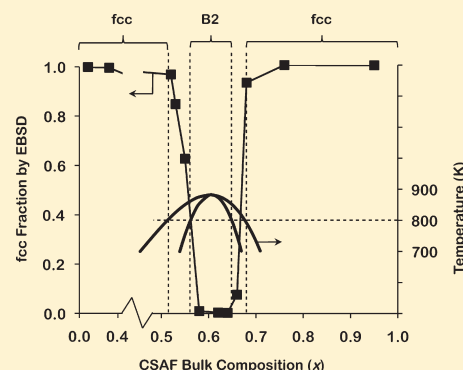
## 1. INTRODUCTION

**1.1. Surface Segregation in Alloys and Other Multicomponent Materials.** Metallic alloys often display properties that are superior to those of their individual components, accounting for their widespread use in applications as diverse as catalysis, corrosion control, and separations. The composition of the alloy surface is a key determinant of processes that take place at the surface. However, the surface composition of an alloy often differs significantly from its bulk composition because of preferential segregation of one component to the surface.[1−19] Thus, characterization of surface segregation is critical to understanding, controlling, and optimizing the properties of alloys relevant to their various applications.

As an example, Pd alloys have been studied extensively as membranes for separation of hydrogen from mixed gas streams such as those encountered in coal and biomass gasification processes.[20−23] In this application, molecular hydrogen dissociatively adsorbs on the membrane surface, producing hydrogen atoms that penetrate and diffuse through the bulk of the membrane. Recombination and desorption of molecular hydrogen on the opposite surface of the membrane results in hydrogen separation with nearly perfect selectivity.[24−28] In this sequence of elementary steps, the *bulk alloy composition* controls the rate of diffusion through the membrane, but the *surface composition*, which differs from bulk composition, determines rate of dissociative hydrogen adsorption.[29−31]

In practical implementation, Pd is alloyed with Cu or Ag to improve mechanical robustness.[27,32−34] Furthermore, alloying of Pd with Cu can impart tolerance to the sulfur containing contaminants commonly found in coal-derived gas streams.[22,35−37] Contamination of the membrane surface by sulfur is one of the critical impediments to the effective implementation of Pd based membranes for hydrogen separation from coal-derived gas mixtures. Thus, understanding surface segregation in $Cu_xPd_{1-x}$ alloys and its impact on sulfur tolerance is important to understanding $Cu_xPd_{1-x}$ alloy performance for hydrogen purification.

Segregation in an alloy such as $Cu_xPd_{1-x}$ is described by the thermodynamic relationship $\theta_{Cu}(x;T,P)$ between the surface composition, $\theta_{Cu}$, and the bulk composition, $x$. Fundamentally, surface segregation results from the balance between the chemical potentials of the atoms in the bulk and those at the surface.[38−40] Thus, surface segregation is a complex function of bulk composition and environmental factors such as temperature, pressure, and the presence of adsorbed species.

A complete description of surface segregation requires that surface composition be understood as a continuous function of bulk composition. Segregation in most alloys has, however, been examined only at a very limited number of discrete compositions.[3,41−43] Surface segregation has been characterized experimentally in a number of binary alloys.[1−5,10,41−47] $Cu_xPd_{1−x}$ alloys have received significant attention from both experimental and computational research groups because of their importance in the hydrogen purification application.[1,2,4,5,22,48] We have reported the experimental characterization of segregation in a polycrystalline $Cu_{0.30}Pd_{0.70}$ alloy, showing that Cu preferentially segregates to the top-surface of the alloy over a wide temperature range, leaving a Cu-depleted subsurface region.[1] Other researchers have reported similar results for the $Cu_{0.50}Pd_{0.50}(110)$[5,44] and $Cu_{0.85}Pd_{0.15}(110)$[45,46] single crystal surfaces. Theoretical studies of $Cu_xPd_{1−x}$ alloys suggest that segregation patterns can vary with bulk composition[12,49,50] and predict a top layer that is Cu-rich with a second layer that is Cu-depleted with respect to the bulk composition.[51,52] We have also shown that adsorption of sulfur onto the $Cu_{0.30}Pd_{0.70}$ surface causes "segregation reversal", creating a top-surface that contains only Pd and S atoms.[2] All prior studies have focused on segregation in $Cu_xPd_{1−x}$ alloys of a single, discrete composition, $x$. Here we report the first application of a high throughput approach to the study of surface segregation in $Cu_xPd_{1−x}$ alloys across a wide, continuous region of the binary alloy composition space, $x = 0.05−0.95$.

**1.2. High Throughput Characterization of Surface Segregation.** The traditional approach for study of segregation over a range of alloy compositions is to prepare and carefully characterize a set of single composition samples. However, even for a binary alloy, this strategy is very time-consuming because of the large number of discrete alloy samples that must be prepared and characterized to sample composition space with high resolution. Because of this challenge, only simulations have, to the best of our knowledge, been applied to the study of segregation over a *continuous* range of bulk composition.[53−55] Efficient experimental characterization of segregation over all possible alloy compositions requires accelerated, parallelized methods of sample preparation and characterization.

To enable high throughput study of segregation and other alloy properties, we have developed tools and methodologies for deposition and characterization of composition spread alloy films (CSAFs). CSAFs are high throughput libraries that contain all possible compositions of a binary (or higher order) alloy deposited onto a single compact substrate.[56−60] Films with lateral composition gradients are formed by depositing alloy components onto substrates from two or more chemically distinct sources. Spatially resolved characterization techniques are used to measure the film's properties as a function of location on the substrate surface, that is, as a function of bulk composition. Having all possible alloy compositions present in one CSAF library allows study of segregation over a continuous range of compositions with a composition resolution that is limited primarily by the spatial resolution of the characterization tools. CSAFs are ideally suited to the study of surface segregation and enable a dramatic increase in the throughput of materials evaluation over conventional studies of a series of single-composition samples.

In this paper, we describe our preparation of $Cu_xPd_{1−x}$ CSAFs on a Mo(110) single crystal substrate using an offset filament deposition tool. We apply electron backscatter diffraction (EBSD) to determine the local structure (bulk phases) of the alloy film as a function of location on the substrate, that is, as a function of bulk alloy composition, $x$. We apply spatially resolved X-ray photoelectron



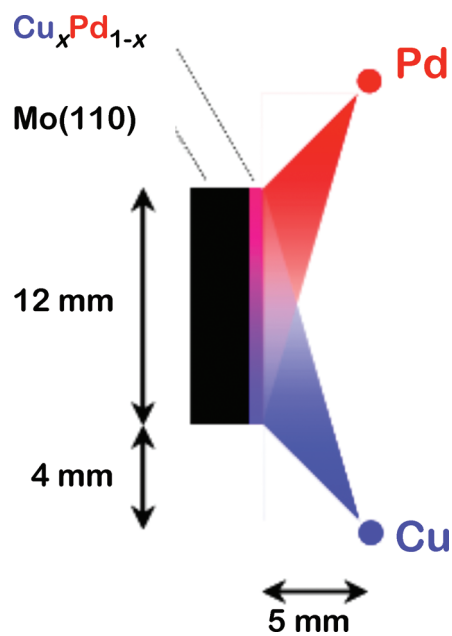**Figure 1.** Schematic diagram of the evaporation geometry used for preparing $Cu_xPd_{1−x}$ CSAFs. The Pd and Cu evaporative line sources (normal to the plane of the figure) are offset from the center of Mo(110) substrate but close enough to create a gradient in flux across the substrate surface.

spectroscopy (XPS) and low energy ion scattering spectroscopy (LEISS) to determine the near-surface composition, $\theta^{ns}_{Cu}(x;T)$, and top-surface composition, $\theta^{top}_{Cu}(x;T)$, of the alloy film as functions of bulk alloy composition, $x$, and temperature, $T$. Finally, we use a simple thermodynamic model to extract enthalpy ($\Delta H_{seg}$) and entropy ($\Delta S_{seg}$) of segregation as functions of bulk composition at temperatures (700−900 K) where the bulk, near-surface, and top-surface are in equilibrium.

## 2. EXPERIMENTAL PROCEDURES

Experiments were carried out in a stainless steel ultrahigh vacuum chamber with a base pressure of $2 \times 10^{-10}$ Torr.[1] The chamber is equipped with a monochromated X-ray source (VG Scientific), a $He^+$ ion gun for LEISS (Specs IQE 12/38), and a hemispherical electron or ion energy analyzer (Specs PHOIBOS 150MCD). In addition, the chamber has an ion gun (Physical Electronics) which was used to sputter clean the substrate surface prior to film deposition. The Mo(110) substrate (12 mm diameter, Monocrystals Company) was attached to a sample holder by spot-welding Ta wires across its back. The sample holder was mounted on a manipulator that allows motion in four degrees of freedom ($x$, $y$, $z$ and $\theta$ rotation about the $z$-axis). The substrate was resistively heated while in thermal contact with a liquid nitrogen reservoir to access a temperature range of 80−1400 K. Once in the chamber, surface carbon was removed by heating the substrate at 1300 K in an atmosphere of oxygen ($\sim 10^{-8}$ Torr) for several hours. After the oxidation process, the Mo(110) substrate was cleaned by repeated cycles of 1 keV $Ar^+$ ion sputtering at 300 K and annealing to 1300 K to remove other impurities to <15% (atomic). Impurities were not detectable by XPS in either the as-deposited or annealed CSAFs.

**2.1. Offset Filament Tool for Deposition of CSAFs.** We have developed an offset filament tool for preparation of CSAFs by

evaporation of metals at high temperatures. We provide a general description of the tool here; design details will be documented in a separate paper. Figure 1 is a schematic diagram of the offset filament concept. Evaporative line sources are made by placing the Cu or Pd evaporant wire in a slot machined into the side of a 3.2 mm diameter × 14 mm long Mo cylinder. These line sources, shown normal to the plane of Figure 1, are located close to the substrate, but offset from its centerline. The sources are positioned opposite one another but shielded from one another to prevent cross-contamination. A type K thermocouple is spot-welded to each source for measuring and controlling the source temperature during deposition. A gradient film is formed on the substrate because of the variation in incident flux across the substrate surface; points closer to the source receive higher evaporant flux than those far from the source. The deposition rate is controlled by the source position relative to the substrate and by the source temperature.

For this work, the offset filament deposition tool was configured with Pd and Cu sources on opposite sides of a 12 mm diameter Mo(110) substrate to create a one-dimensional, $Cu_xPd_{1-x}$ CSAF. Mo was chosen as a substrate to minimize the potential for interdiffusion between substrate and film components.[61,62] The CSAF was prepared by codepositing the two components to generate a film with a thickness of ~100 nm. A thickness of 100 nm was chosen to ensure film stability during heating; thinner films were observed to dewet from the substrate when annealed at 900 K.

A related technique for depositing $Cu_xPd_{1-x}$ CSAFs, based on magnetron cosputtering of Cu and Pd components, has recently been reported by Westerwaal and co-workers.[63] In that work, CSAFs were prepared as model hydrogen separation materials and examined for their hydrogenation behavior using a high-throughput optical hydrogenography technique.

**2.2. Characterization of CSAF Surface Composition and Local Bulk Structure.** X-ray photoelectron spectroscopy (XPS) was used to characterize the near-surface (~7 atomic layers) composition, $\theta_{Cu}^{ns}$, of the $Cu_xPd_{1-x}$ CSAF. XPS measurements used Al Kα radiation from a monochromated X-ray source focused on a small region of the sample. The X-ray spot is elliptical with a minor axis (~600 $\mu$m) parallel to the composition gradient of the CSAF. The X-rays were incident at an angle of 25° from the substrate normal. The analyzer was operated at a pass energy of 100 eV and collected electrons photoemitted at an angle of 30° from the substrate normal. All XPS measurements were performed at room temperature, at which the near-surface composition determined by XPS is stable over the time scale of the measurement (~3 min). The Pd $3d_{5/2}$ and Cu $2p_{3/2}$ photoemission features at binding energies of 335 and 933 eV, respectively, were used for quantitative estimates of $\theta_{Cu}^{ns}$ of the CSAFs. The Mo $3d_{5/2}$ signal at 228 eV was also monitored during deposition of the films. Quantitative estimates of $\theta_{Cu}^{ns}$ were made from Cu and Pd XPS signal intensities ($I_{Cu}$ and $I_{Pd}$) normalized by calibration signals obtained from pure component films, $I_{Cu}^\infty$ and $I_{Pd}^\infty$. Thus, the Cu mole fraction in the near-surface region is given by

$$\theta_{Cu}^{ns} = \frac{I_{Cu}/I_{Cu}^\infty}{\left(I_{Cu}/I_{Cu}^\infty\right) + \left(I_{Pd}/I_{Pd}^\infty\right)} \qquad (1)$$

On the basis of the results of repeated measurements performed on multiple films at similar bulk compositions, $x$, the values of $\theta_{Cu}^{ns}$ measured by XPS are reproducible to within ±3%.

Low energy ion scattering spectroscopy (LEISS) was used to characterize the composition of the topmost atomic layer of the $Cu_xPd_{1-x}$ CSAF, $\theta_{Cu}^{top}$. LEISS experiments used He$^+$ ions at $E_0$ = 750 eV

with a beam spot size of ~800 $\mu$m. He$^+$ ions were incident at an angle of 40° from the substrate normal, and the scattered ions were collected at an angle of 60° from the substrate normal. A low incident ion current of ~50 nA with a scan time of ~50 s per spectrum was used to minimize the potential for sputter damage by incident He$^+$. Significantly higher currents could alter the top-surface composition. The top-surface composition was determined by comparing the Pd and Cu LEISS peak intensities obtained from the alloy film with LEISS peak intensities measured from pure component films. For quantitative estimates of the top-surface composition, the LEISS features at $E/E_0$ = 0.89 for Cu and $E/E_0$ = 0.93 for Pd were used. The reproducibility of the values of $\theta_{Cu}^{top}$ measured by LEISS on multiple films at similar bulk compositions, $x$, is estimated to be within ±5%.

Electron backscatter diffraction (EBSD) was used to determine the local distribution of crystal structures in the $Cu_xPd_{1-x}$ CSAF. Measurements were performed in a Quanta 200 scanning electron microscope (FEI, Inc.) equipped with an orientation imaging microscopy (OIM) system (EDAX, Inc.). The EBSD patterns were acquired at an operating voltage of 20 kV, with the sample surface normal tilted 70° from the incident electron beam. Beam size was <4 nm, lateral resolution was ~20 nm, and sampling depth was ~10−20 nm. Commercial OIM software (EDAX, Inc.) was used to record and index the EBSD patterns. Indexing was limited to B2 (an intermetallic phase derived from the bcc structure) and fcc phases. OIM is generally insensitive to the small lattice parameter differences between fcc-copper and fcc-palladium. A grain size dilation correction was applied to filter noise from the orientation and phase maps. The analysis was done at 12 different bulk compositions, $x$, that is, 12 positions on the substrate. At each location, an area of ~12 $\mu$m × 12 $\mu$m was scanned with a step size of 0.1 $\mu$m; acquisition time for each scan was ~20 min.

## 3. RESULTS

**3.1. Deposition of $Cu_xPd_{1-x}$ CSAFs.** The first step in quantitative preparation of the CSAFs is measurement of Cu and Pd deposition rates at various points across the substrate surface. A pure, variable thickness Cu film was grown by evaporating Cu onto the clean Mo(110) substrate from a Cu line source held at 1230 K. The substrate was at 300 K at the start of deposition, and its temperature increased by ~50 K during deposition. Figure 2 shows the results of XPS characterization of Cu film growth as functions of both location on the substrate and deposition time. At the shortest deposition time (4 min), the Cu $2p_{3/2}$ XPS signal decreased monotonically across the substrate face as the distance from the source filament increased. At the same time, the Mo $3d_{5/2}$ signal, which had been constant across the face of the clean substrate, was attenuated. As the deposition time increased, the Cu $2p_{3/2}$ signal grew and the Mo $3d_{5/2}$ signal was suppressed further. At the longest deposition time shown (19 min), the Cu $2p_{3/2}$ signal saturates and the Mo $3d_{5/2}$ signal disappears at the edge of the substrate nearest the source. After this deposition time, the thickness of the Cu film near the source had approached the mean free path of the Cu $2p_{3/2}$ and Mo $3d_{5/2}$ photoelectrons, 1.08 and 1.92 nm, respectively.[64] The spatial and temporal variations in the Cu $2p_{3/2}$ and Mo $3d_{5/2}$ signals during Cu deposition clearly point to the formation of a Cu film with a thickness decreasing monotonically with distance from the Cu line source.

The time dependence of the Cu $2p_{3/2}$ and Mo $3d_{5/2}$ XPS signals can be used to quantitatively determine the deposition rates at any point on the substrate surface. Figure 3 is a plot of the Cu $2p_{3/2}$ and Mo $3d_{5/2}$ signals at the midpoint of the substrate as functions of deposition time. The Cu film deposition rate can be
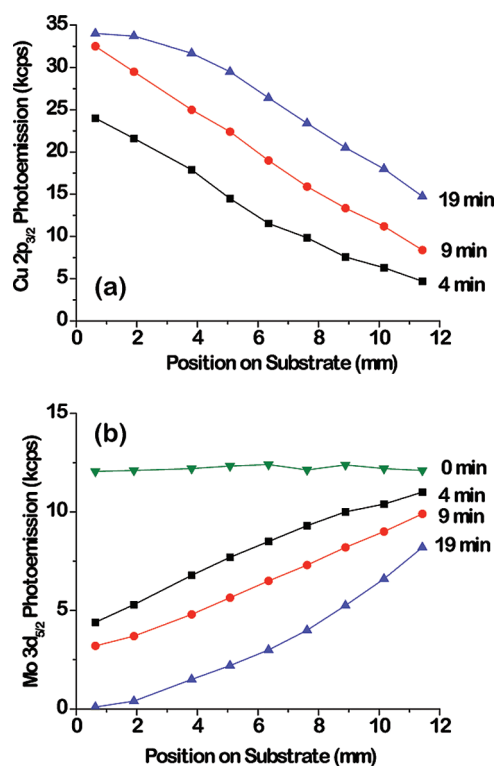
C

dx.doi.org/10.1021/jp201793d |J. Phys. Chem. C XXXX, XXX, 000–000

**Figure 2.** (a) Cu 2p$_{3/2}$ and (b) Mo 3d$_{5/2}$ XPS signals as functions of position across the Mo(110) substrate following Cu deposition for 0, 4, 9, and 19 min. The Cu 2p$_{3/2}$ signal growth is accompanied by attenuation of the Mo 3d$_{5/2}$ signal. The gradients in the Cu 2p$_{3/2}$ and Mo 3d$_{5/2}$ signal intensities clearly indicate growth of the Cu film at different rates across the substrate.
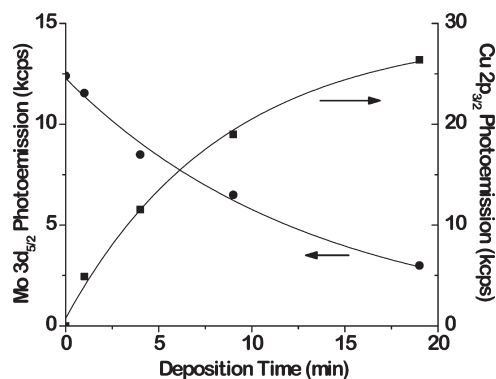


**Figure 3.** Cu 2p$_{3/2}$ and Mo 3d$_{5/2}$ XPS signals at the center of the Mo(110) substrate as a function of deposition time. The solid lines represent the exponential fits to the Cu growth and Mo decay curves.

estimated by analyzing either the Cu or the Mo data. The expression that describes growth of the Cu 2p$_{3/2}$ XPS signal is

$$I_{Cu} = I_{Cu}^{\infty}\left[1 - \exp\left(\frac{-r_{Cu}t}{\lambda_{Cu}\cos\theta}\right)\right] \quad (2)$$

where $I_{Cu}$ is the Cu 2p$_{3/2}$ XPS intensity, $I_{Cu}^{\infty}$ is the intensity observed from pure (infinitely thick) Cu, $t$ is the deposition time, $\lambda_{Cu} = 1.08$ nm is the mean free path of Cu 2p$_{3/2}$ photoelectrons in Cu,[64] $\theta$ is the angle at which the analyzer collects the emitted photoelectrons, and $r_{Cu}$ is the Cu deposition rate.[64] The best fit
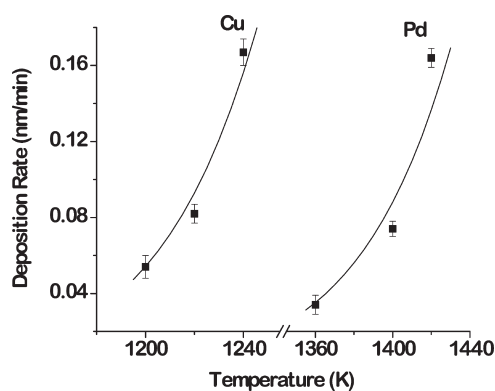


**Figure 4.** Cu and Pd deposition rates measured at the center of the Mo(110) substrate as a function of deposition source temperature. The lines represent fits of the Hertz-Knudsen equation to the data. For codeposition, source temperatures are typically controlled to give equal deposition rates at the center of the substrate.

of eq 2 to the data in Figure 3, shown as the solid line, corresponds to a Cu deposition rate of $r_{Cu} = 0.111 \pm 0.015$ nm/min. The corresponding expression for attenuation of the Mo 3d$_{5/2}$ signal is

$$I_{Mo} = I_{Mo}^{\infty}\exp\left(\frac{-r_{Cu}t}{\lambda_{Mo}\cos\theta}\right) \quad (3)$$

where $I_{Mo}$ is the Mo 3d$_{5/2}$ XPS intensity, $I_{Mo}^{\infty}$ is the intensity from the clean Mo substrate, and $\lambda_{Mo} = 1.92$ nm is the mean free path of Mo 3d$_{5/2}$ photoelectrons in Cu.[64] The best fit of the Mo XPS signals to this expression, shown as the solid line in Figure 3, corresponds to a deposition rate of $r_{Cu} = 0.125 \pm 0.008$ nm/min. In a similar manner, the deposition rates for the Cu and Pd films were estimated at several locations across the substrate.

The deposition rates can be controlled by changing evaporation geometry or by changing the temperature of the evaporative sources. Figure 4 shows the impact of source temperature on deposition rates of both Cu and Pd at the center of the Mo(110) substrate using the deposition geometry shown in Figure 1. The solid line in Figure 4 represents the deposition rates for Cu and Pd as a function of temperature estimated by fitting the Hertz Knudsen equation to the data.[65−67] The deposition rates of both evaporants increase with temperature, as expected. To achieve similar Pd and Cu deposition rates at the center of the substrate, the Pd source must be held at a higher temperature than the Cu source, consistent with the higher heat of vaporization of Pd (362 kJ/mol vs 300.4 kJ/mol).[68] The bulk composition of the film, $x$, at each point across the substrate was calculated from the local deposition rate of the film components:

$$x = \frac{r_{Cu}\rho_{Cu}}{r_{Cu}\rho_{Cu} + r_{Pd}\rho_{Pd}} \quad (4)$$

where $r_{Cu}$ and $r_{Pd}$ are the deposition rates of Cu and Pd, respectively, at any position on the substrate, and $\rho_{Cu}$ and $\rho_{Pd}$ are the molar densities of Cu and Pd, respectively.

In this work, 100 nm thick Cu$_x$Pd$_{1-x}$ CSAFs were prepared by codepositing opposing Cu and Pd gradients onto the Mo(110) substrate at 300 K. A thickness of 100 nm was chosen because significantly thinner films were observed to dewet during heating. Furthermore, 100 nm is sufficiently thick that segregation to the CSAF surface will not significantly deplete the bulk CSAF composition. To maximize the range of bulk compositions, $x$,
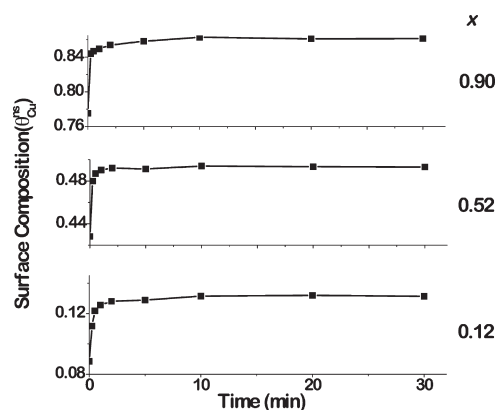
D

dx.doi.org/10.1021/jp201793d |J. Phys. Chem. C XXXX, XXX, 000–000

**Figure 5.** Near-surface (XPS) composition of a 100 nm thick $Cu_xPd_{1-x}$ CSAF as a function of anneal time at 800 K for three different values of the bulk composition. Steady state compositions are reached within 10 min, evidence that the near-surface is in equilibrium with the bulk.



**Figure 6.** (a) EBSD orientation maps acquired at three bulk compositions of a 100 nm thick $Cu_xPd_{1-x}$ CSAF that was first annealed at 800 K and then cooled to room temperature. The crystallographic triangle represents the color code for grain orientation; (111) orientation (blue), preferred in the fcc phase, dominates at $x = 0.09$ and 0.95. (b) Phase maps derived from the composition maps confirm fcc structure (red) at high and low $x$, and B2 structure (green) at $x = 0.62$.

in the $Cu_xPd_{1-x}$ CSAF, the Pd and Cu line sources were operated at temperatures that deliver similar deposition rates at the center of the substrate. Thus, films were deposited with the Cu source operated at 1230 K and the Pd source operated at 1415 K. These conditions gave a composition range of $x = 0.05-0.95$ across the $Cu_xPd_{1-x}$ CSAF. We used the 100 nm CSAF to study segregation in $Cu_xPd_{1-x}$ as a function of bulk composition and temperature.

As-deposited CSAFs were annealed to equilibrate their near-surface compositions, $\theta_{Cu}^{ns}$, measured by XPS, and bulk compositions, $x$. Figure 5 shows the near-surface composition of a 100 nm $Cu_xPd_{1-x}$ CSAF at three different bulk compositions, $x$ (i.e., three different locations on the substrate), as a function of annealing time at 800 K. The first point in each series is $\theta_{Cu}^{ns}$ of the film at that bulk composition as prepared at 300 K. For each bulk composition, $\theta_{Cu}^{ns}$ achieves a steady state value after annealing for 10 min. Similar experiments show that steady state compositions are also reached within 10 min during annealing at 700 and 900 K. These results are consistent with those we previously reported for a polycrystalline $Cu_{0.30}Pd_{0.70}$ sample, which showed that annealing at temperatures ≥ 700 K for periods of >15 min is sufficient to equilibrate the near-surface region with the bulk.[1] We note that the impact of lateral diffusion on CSAF composition is insignificant. The spatial resolution across the CSAF that we typically select for analysis is on the order of 100 $\mu$m, $10^3$ times larger than the thickness of the CSAF. Thus, the time required for any arbitrary concentration change over the two length scales differs by a factor of $10^6$. Our XPS data confirm that the CSAF lateral composition is stable over the time scales of our experiments. After initial rapid equilibration of concentrations normal to the surface, concentrations at specific locations on the CSAF remain stable for at least one hour (only the first 30 min of an hour-long experiment are shown in Figure 5).

**3.2. Characterization of CSAF Local Structure.** Prior to the study of segregation in a CSAF, the bulk structure of the equilibrated film must be determined for comparison to that of the bulk phase diagram of the alloy system under study. The structure of a thin alloy film can differ from that of the bulk material and, in principle, may influence segregation to the surface. Equally importantly, the texture or surface orientation of the grains forming the film can also influence segregation to the surface. Thus,
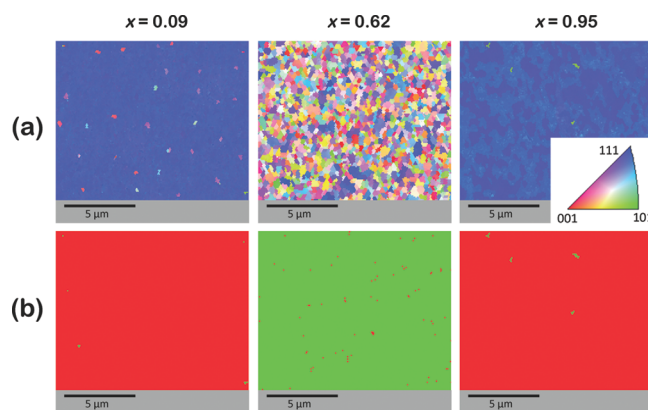
understanding the film texture as a function of local bulk composition, $x$, may provide insight into the nature of segregation.

The phase diagram for bulk CuPd reveals the existence of multiple phases with fcc or B2 bulk structures.[69] At temperatures above 875 K, the alloy has a fcc structure across the entire composition space, $x = 0-1$. As the temperature is lowered, a B2 phase appears at $x = 0.60$. The composition region over which the B2 phase exists grows as the temperature is decreased further. At 800 K, the CuPd phase diagram has five regions: fcc for $x < 0.51$, mixed fcc and B2 for $0.51 < x < 0.56$, B2 for $0.56 < x < 0.65$, mixed fcc and B2 for $0.65 < x < 0.68$, and then fcc again for $x > 0.68$. In principle, the segregation properties of the $Cu_xPd_{1-x}$ alloy are sensitive to the bulk phase of the alloy and this might be explored by studies of segregation at the surface of the $Cu_xPd_{1-x}$ CSAF.

EBSD was used to characterize the structure and crystallographic texture of a 100 nm thick $Cu_xPd_{1-x}$ CSAF that was first equilibrated by annealing at 800 K and then cooled to room temperature. EBSD images of the $Cu_xPd_{1-x}$ CSAF were acquired at 12 different compositions ranging from $x = 0.09$ to 0.95. Orientation maps for three of the 12 compositions are shown in Figure 6a. The colors in the figure represent the different grain orientations in the fcc and B2 phases; blue, red, and green correspond to (111), (001), and (101) orientations, respectively, as represented by the crystallographic triangle (inset). At both high ($x = 0.95$) and low ($x = 0.09$) bulk Cu composition, grains are preferentially oriented near the (111) direction (blue), which is expected for the fcc phase. In contrast, at intermediate bulk Cu content ($x = 0.62$), grains are randomly oriented. Figure 6b shows the phase maps derived from the orientaion data. The fcc phase (red) cleay dominates at $x = 0.09$ and 0.95; B2 (green) dominates at $x = 0.62$.

Figure 7 compares the film structure, calculated from the phase maps obtained at each of the 12 compositions across the film's surface, to the bulk structure at 800 K as reported in the published CuPd phase diagram. We note that while the effective temperature at which the structure of the CSAF has been frozen in during cooling is not well-defined, it must be <800 K. Nonetheless, the structures determined by EBSD reveal the presence of the B2 region and the two-phase regions at exactly the compositions
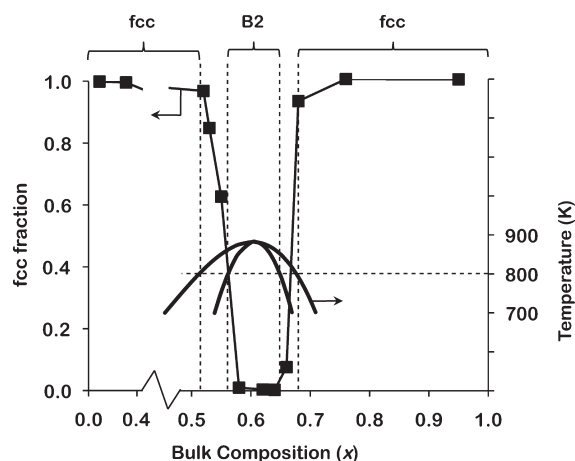
**Figure 7.** Film structure, calculated from phase maps obtained from the CSAF described in Figure 6, as a function of bulk composition, $x$. The bulk CuPd phase diagram (between 700 and 900 K) appears as curved lines;[68] locations of phase boundaries at 800 K are highlighted as dotted lines. EBSD measurements of CSAF structure match the bulk phase diagram.

expected on the basis of the CuPd phase diagram. This implies that our calibration of the CSAF composition is quite accurate, probably within 2%. Furthermore, this EBSD data demonstrates that the bulk structure of the 100 nm thick CSAF is that of the bulk $Cu_xPd_{1-x}$ alloy, thus illustrating the potential of the CSAF platform for high-throughput determination of phase diagrams.

**3.3. Characterization of CSAF near-Surface and Top-Surface Composition.** A second 100 nm thick $Cu_xPd_{1-x}$ CSAF was prepared, and its near-surface and top-surface compositions were characterized over a range of bulk compositions (i.e., location on the substrate) and temperatures. Figure 8a shows the CSAF near-surface composition, $\theta_{Cu}^{ns}$, measured using XPS, as a function of bulk composition, $x$. Near-surface composition was measured at room temperature ($\sim$300 K) after annealing the film at the specified temperature (300−900 K) for 20 min. $\theta_{Cu}^{ns}$ of the as-prepared film (■) is less than the corresponding bulk composition at all $x$, indicating depletion of Cu in the near-surface region of the film. The extent of Cu depletion is greatest near $x = 0.85$, and it diminishes as x approaches both 0 and 1—at locations physically near the Pd and Cu sources. It is likely that substrate temperature is slightly higher near the hot sources, enabling diffusion of the Cu component to the surface to begin during deposition. Upon annealing at 500 K (●) and 700 K (▲), the Pd and Cu film components interdiffuse and $\theta_{Cu}^{ns}$ increases, approaching the bulk composition, $x$, over the entire range of bulk composition. Upon annealing at 800 K (not shown) and 900 K, $\theta_{Cu}^{ns}$ does not change significantly from its value at 700 K, remaining slightly less than the bulk composition over the entire composition range of the $Cu_xPd_{1-x}$ CSAF.

The composition of the topmost layer of the CSAF was measured using LEISS. Our previous study of surface segregation in a single composition $Cu_{0.30}Pd_{0.70}$ alloy revealed that the composition of the top-surface is very sensitive to analysis temperature, and changes reversibly with temperature on time scales of a few minutes, independent of whether the sample was heated or cooled to the analysis temperature.[1] Thus, after annealing the film at 900 K for 20 min, LEIS spectra were acquired at number of locations across the CSAF surface (i.e., bulk compositions, $x$), over a range of temperatures from 300 to 900 K. Figure 8b shows the top-surface composition, $\theta_{Cu}^{top}$, of a 100 nm



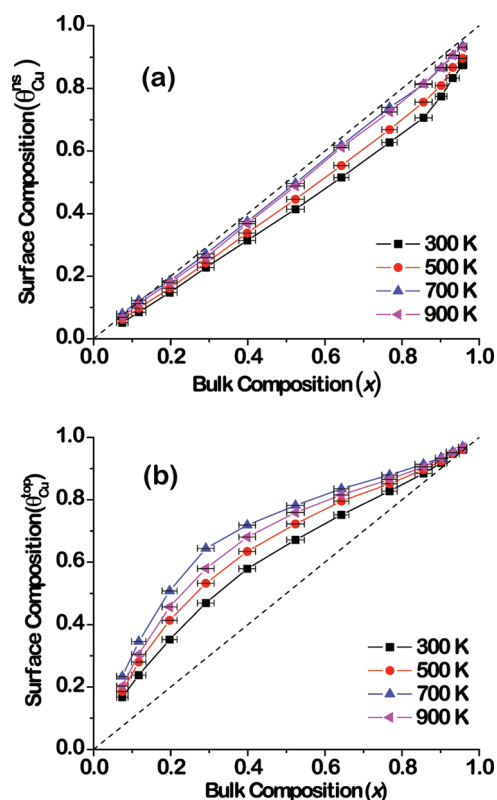**Figure 8.** (a) Near-surface (XPS) and (b) top-surface (LEISS) compositions of a 100 nm thick $Cu_xPd_{1-x}$ CSAF as functions of bulk composition, $x$, following annealing at various temperatures. The near-surface composition was measured at 300 K using XPS after annealing at the specified temperature for 20 min. The near-surface of the as-prepared film is slightly Pd rich at all $x$; annealing induces diffusion of Cu into the near-surface. The top-surface composition was measured using LEISS at the temperature specified after annealing at 900 K for 20 min. The top-surface of the film is Cu-rich at all temperatures.

thick $Cu_xPd_{1-x}$ CSAF, as a function of bulk composition, $x$. At each characterization temperature, $\theta_{Cu}^{top}$ varies smoothly with $x$; we observed similar behavior for 100 nm thick CSAFs annealed at 800 K (not shown). As shown in the Figure, $\theta_{Cu}^{top}$ at 300 K (■) is significantly higher than the bulk composition, $x$, at all bulk compositions. At 500 K (●) and 700 K (▲), $\theta_{Cu}^{top}$ increases over the entire range of bulk compositions. The values of $\theta_{Cu}^{top}$ then *decrease* slightly at 900 K (left triangle).

To highlight the dependence of $\theta_{Cu}^{top}$ on temperature, Figure 9 displays the top-surface composition data from Figure 8b as a function of temperature. At each bulk composition, $\theta_{Cu}^{top}$ exhibits a maximum at $\sim$700 K. For an alloy surface at thermodynamic equilibrium with the bulk, such maxima may reflect a change from order driven segregation in the low temperature regime to disorder driven segregation in the high temperature regime.[38] Our observation of Cu segregation to the topmost layer of $Cu_xPd_{1-x}$ alloys, and its temperature dependence, is consistent with prior experimental characterization of segregation in single composition samples, including our own for $Cu_{0.30}Pd_{0.70}$.[1,5,45]

## 4. DISCUSSION

Analysis of the near-surface and top-surface compositions of a 100 nm thick $Cu_xPd_{1-x}$ CSAF using spatially resolved XPS and LEISS has enabled high throughput characterization of surface
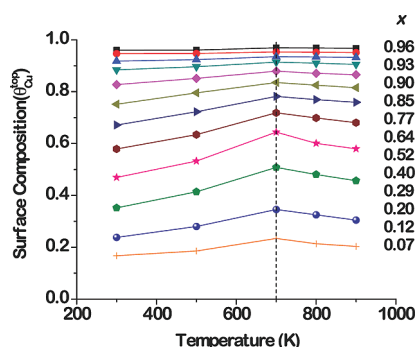
**Figure 9.** Top-surface Cu compositions as functions of temperature at different bulk $Cu_xPd_{1-x}$ CSAF compositions, $x$. The CSAF was annealed at 900 K for 20 min for equilibration, followed by measurement of the top layer composition using LEISS over a range of temperatures. For all $x$, top-surface Cu concentration exhibits a maximum at 700 K.
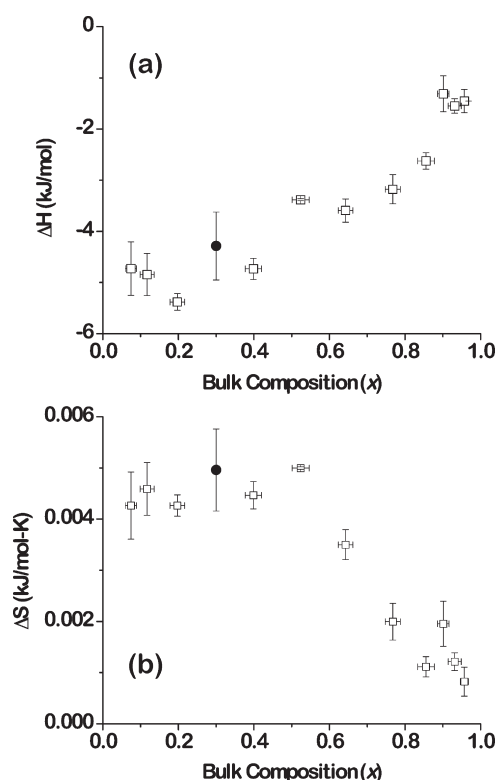


**Figure 10.** (a) $\Delta H_{seg}$ and (b) $\Delta S_{seg}$ as functions of bulk composition for a 100 nm thick $Cu_xPd_{1-x}$ CSAF. $\Delta H_{seg}$ and $\Delta S_{seg}$ were determined by applying the Langmuir–McLean isotherm to the data in Figure 7. $\Delta H_{seg}$ and $\Delta S_{seg}$ determined from a $Cu_{0.30}Pd_{0.70}$ sample is represented by the solid symbol (●).[1] The approach of $\Delta H_{seg}$ and $\Delta S_{seg}$ toward zero as the bulk composition approaches $x = 1$ is consistent with the tendency of the alloy toward ideal behavior at $x = 1$.

segregation, spanning alloy composition space from $x = 0.05$ to 0.95. The components of the $Cu_xPd_{1-x}$ CSAF were codeposited at 300 K. Annealing the film at temperatures from 700 to 900 K causes the components to interdiffuse and allows the surface composition to equilibrate with the bulk composition. As illustrated in Figures 8 and 9, the topmost layer is rich in Cu across the entire alloy composition range and at temperatures from 300 to 900 K. This result is consistent with the fact that the surface

energy of Cu $(1.83 \text{ J/m}^2)$ is lower than that of Pd $(2.05 \text{ J/m}^2)$.[70] The extent of Cu segregation to the topmost layer is greatest at low bulk Cu content, $x$; alloy behavior approaches that of an ideal mixture, $\theta_{Cu}^{top} = x$, as the bulk Cu composition approaches $x = 1$.

One point of possible relevance to the study of segregation in the $Cu_xPd_{1-x}$ is that a phase transition occurs within the composition range $x = 0.05-0.95$. As indicated by the dotted lines in Figure 7, at 800 K, the bulk $Cu_xPd_{1-x}$ alloy displays fcc structure in the ranges $x = 0.00-0.51$ and $x = 0.68-1.00$, and B2 structure in the range $0.56 < x < 0.65$. The intermediate regions contain both phases.[69] At temperatures below 800 K, the B2 range is wider, and at higher temperatures the B2 range narrows until the alloy exists only in the fcc phase for $T > 875$ K. Our EBSD results show that the expected phase changes do take place across the CSAF. However, the effect of phase changes is not reflected in our measurements of either the top-surface or the near-surface compositions (Figure 8), both of which vary smoothly with film composition, $x$. This result indicates that segregation is insensitive to bulk structure.

Segregation is a thermodynamic property of an alloy. In other words, the composition of the topmost layer is a thermodynamic function of the bulk alloy composition, temperature, and pressure (weak), $\theta_{Cu}^{top}(x;T,P)$. An important goal of this work is to determine this function over a significant range of bulk composition. In the energy-driven temperature regime, $\geq 700$ K, equilibrium segregation can be described by the Langmuir–McLean formulation of the Gibbs isotherm:[38,42,71-73]

$$\frac{\theta_{Cu}^{top}}{\theta_{Pd}^{top}} = \frac{x_{Cu}^{bulk}}{x_{Pd}^{bulk}} \exp\left(\frac{-\Delta G_{seg}}{RT}\right)$$

$$\frac{\theta_{Cu}^{top}}{(1 - \theta_{Cu}^{top})} = \frac{x}{(1-x)} \exp\left(\frac{-\Delta G_{seg}}{RT}\right)$$

$$\frac{\theta_{Cu}^{top}}{(1 - \theta_{Cu}^{top})} = \frac{x}{(1-x)} \exp\left(\frac{-\Delta H_{seg}}{RT} + \frac{\Delta S_{seg}}{R}\right) \quad (5)$$

In this equation, $\Delta G_{seg}$, $\Delta H_{seg}$, and $\Delta S_{seg}$ are the free energy, enthalpy, and entropy of segregation for Cu, respectively. $\Delta G_{seg}$ is usually described as having contributions from the difference in the surface free energy of the two components, strain effects arising from different atomic sizes, and the interactions between the two components.[38,40,71]

The thermodynamic quantities that describe segregation of Cu to the topmost atomic layer of the $Cu_xPd_{1-x}$ alloy can be determined from the temperature dependence of the top-surface compositions, illustrated in Figure 9. Figure 10 shows $\Delta H_{seg}$ (a) and $\Delta S_{seg}$ (b) as functions of bulk composition, estimated by application of the Langmuir–McLean equation to segregation data for $T \geq 700$ K. Consistent with the observed preferential segregation of Cu to the top-surface, $\Delta H_{seg}$ is negative over the entire range of bulk compositions. At the lowest bulk Cu contents, $\Delta H_{seg}$ is relatively insensitive to bulk composition, possibly due to fewer opportunities for interaction among Cu atoms. As the bulk alloy composition approaches $x = 1$, both $\Delta H_{seg}$ and $\Delta S_{seg}$ tend toward zero, reflecting the approach of the alloy to ideal behavior ($\theta_{Cu}^{top} \sim x$, Figure 8b) at the highest bulk Cu concentrations. The values of $\Delta H_{seg}$ and $\Delta S_{seg}$ near $x \sim 0.3$ are consistent with those of our previous chracterization of segregation on a single composition $Cu_{0.30}Pd_{0.70}$ sample, represented by the solid circle (●) in Figure 10a and b.[1] The ability to use the $Cu_xPd_{1-x}$ CSAF to successfully replicate segregation measurements made on a bulk material illustrates the value of the CSAF

G

dx.doi.org/10.1021/jp201793d |J. Phys. Chem. C XXXX, XXX, 000–000

sample library for high-throughput characterization of segregation behavior in alloys across composition space.

While many other researchers have reported segregation of Cu to the surfaces of CuPd alloys in vacuum,[5,44−46] few have used their data to estimate the thermodynamic parameters $\Delta H_{seg}$ and $\Delta S_{seg}$. Two mid-1980s studies described application of Auger spectroscopy and XPS for characterization of segregation and estimation of the thermodynamic parameters for polycrystalline $\sim$Cu$_{90}$Pd$_{10}$ samples.[10,74] Consistent with our results, both groups reported preferential segregation of Cu to the alloy surface. However, using an approach similar to the one we describe, both groups extracted *positive* $\Delta H_{seg}$; we estimate −2 kJ/mol in the same composition region (Figure 10a). (In these papers, $\Delta H_{seg}$ is reported with respect to Pd segregation and is negative; for comparison with our figures, which are with respect to Cu segregation, the sign must be reversed.) The reasons for the difference are unclear. However, we note that one of these reports includes a calculation of $\Delta H_{seg}$ performed by summing contributions of component surface free energy, energy of mixing, and lattice strain.[74,75] The result of the calculation for Cu$_{90}$Pd$_{10}$ is −3 kJ/mol, which compares well with our measurement.

## 5. CONCLUSION

A novel offset filament deposition tool was used to deposit CSAFs for the study of surface segregation in the Cu$_x$Pd$_{1−x}$ system throughout a composition space continuum between $x = 0.05$ and 0.95. EBSD characterization showed that the local structure across the Cu$_x$Pd$_{1−x}$ CSAF matched that of the published phase diagrams for bulk CuPd. The near-surface and bulk compositions of a 100 nm thick Cu$_x$Pd$_{1−x}$ CSAF attain equilibrium on annealing at temperatures in the range 700 to 900 K. Preferential segregation of Cu to the top-surface of the CSAF was observed at all bulk compositions. The Langmuir−McLean thermodynamic model was applied to estimate the enthalpy, $\Delta H_{seg}$, and entropy, $\Delta S_{seg}$, of segregation as a function of bulk Cu$_x$Pd$_{1−x}$ composition, for $x = 0.05−0.95$. At $x \sim 0.30$, CSAF segregation results compare well with those previously reported for a bulk, polycrystalline Cu$_{0.30}$Pd$_{0.70}$ alloy. Surface compositions varied smoothly with bulk CSAF bulk composition, suggesting that segregation is insensitive to changes in the local structure of the alloy. Our results demonstrate the utility of the CSAF platform as a high throughput sample library for study of surface segregation and structure of multicomponent materials.

## ■ AUTHOR INFORMATION

**Corresponding Author**
*E-mail: jbmiller@andrew.cmu.edu.

## ■ ACKNOWLEDGMENT

## ■ REFERENCES

(1) Miller, J. B.; Matranga, C.; Gellman, A. J. *Surf. Sci.* **2008**, *602*, 375.
(2) Miller, J. B.; Morreale, B. D.; Gellman, A. J. *Surf. Sci.* **2008**, *602*, 1819.
(3) Yi, C. W.; Luo, K.; Wei, T.; Goodman, D. W. *J. Phys. Chem. B* **2005**, *109*, 18535.
(4) Loboda-Cackovic, J. *Vacuum* **1997**, *48*, 913.
(5) Loboda-Cackovic, J.; Mousa, M. S.; Block, J. H. *Vacuum* **1995**, *46*, 89.
(6) Loboda-Cackovic, J.; Block, J. H. *Vacuum* **1995**, *46*, 1449.
(7) Novacek, P.; Liegl, A.; Vonbank, M.; Borrell, M.; Hofer, W.; Varga, P. *Fresenius' Z. Anal. Chem.* **1989**, *333*, 453.
(8) Weigand, P.; Novacek, P.; Husen, G. v.; Neidhart, T.; Varga, P. *Surf. Sci.* **1992**, *269*, 1129.
(9) Vasiliev, M. A. *J. Phys. D: Appl. Phys.* **1997**, *30*, 3037.
(10) Kumar, T. S. S.; Hegde, H. S. *Appl. Surf. Sci.* **1985**, *20*, 290.
(11) Bennett, R. A.; Poulston, S.; Price, N. J.; Reilly, J. P.; Stone, P.; Barnes, C. J.; Bowker, M. *Surf. Sci.* **1999**, *433*, 816.
(12) Gallis, C.; Legrand, B.; Saul, A.; Treglia, G.; Hecquet, P.; Salanon, B. *Surf. Sci.* **1996**, *352*, 588.
(13) Hoffmann, M. A.; Wynblatt, P. *Metall. Mater. Trans. A* **1991**, *22*, 1833.
(14) Hoffmann, M. A.; Wynblatt, P. *Metall. Mater. Trans. A* **1991**, *22*, 1841.
(15) Moison, J. M.; Guille, C.; Houzay, F.; Barthe, F.; Rompay, M. V. *Phys. Rev. B* **1989**, *40*, 6149.
(16) Moison, J. M.; Houzay, F.; Barthe, F.; Gerard, J. M.; Jusserand, B.; Massies, J.; Turcosandroff, F. S. *J. Cryst. Growth* **1991**, *111*, 141.
(17) Tian, X.; Fu, R. K. Y.; Wang, L.; Chu, P. K. *Mater. Sci. Eng., A* **2001**, *316*, 200.
(18) Pop, D.; Wolski, K. *Appl. Surf. Sci.* **2006**, *253*, 2244.
(19) Kumar, V.; Kumar, D.; Joshi, S. K. *Phys. Rev. B* **1979**, *19*, 1954.
(20) Zhang, X.; Xiong, G.; Yang, W. *Stud. Surf. Sci. Catal.* **2007**, *167*, 219.
(21) Nam, S. E.; Seong, Y. K.; Lee, J. W.; Lee, K. H. *Desalination* **2009**, *236*, 51.
(22) Kamakoti, P.; Morreale, B. D.; Ciocco, M. V.; Howard, B. H.; Killmeyer, R. P.; Cugini, A. V.; Sholl, D. S. *Science* **2005**, *307*, 569.
(23) Roa, F.; Way, J. D.; McCormick, R. L.; Paglieri, S. N. *Chem. Eng. J.* **2003**, *93*, 11.
(24) Ma, Y. H.; Engwall, E. E.; Mardilovich, I. P. *Fuel Chem. Div. Repr.* **2003**, *48*, 333.
(25) Brenner, J. R.; Bhagat, G.; Vasa, P. *Int. J. Oil, Gas Coal Technology* **2008**, *1*, 109.
(26) Caga, I. T.; Winterbottom, J. M. *Catal. Lett.* **1989**, *3*, 309.
(27) Foletto, E. L.; Silveira, J. V. W. D.; Jahn, S. L. *Lat. Ame. Appl. Res.* **2008**, *38*, 79.
(28) Hughes, D. T.; Harris, I. R. *J. Less-Common Met.* **1978**, *61*, 9.
(29) Howard, B. H.; Killmeyer, R. P.; Rothenberger, K. S.; Cugini, A. V.; Morreale, B. D.; Enick, R. M.; Bustamante, F. *J. Membr. Sci.* **2004**, *241*, 207.
(30) Morreale, B. D.; Ciocco, M. V.; Enick, R. M.; Morsi, B. I.; Howard, B. H.; Cugini, A. V.; Rothenberger, K. S. *J. Membr. Sci.* **2003**, *212*, 87.
(31) Kamakoti, P.; Morreale, B. D.; Ciocco, M. V.; Howard, B. H.; Killmeyer, R. P.; Cugini, A. V.; Sholl, D. S. *Science* **2005**, *307*, 569.
(32) Gade, S. K.; Thoen, P. M.; Way, J. D. *J. Membr. Sci.* **2008**, *316*, 112.
(33) Tong, H. D.; Gielens, F. C.; Hoang, H. T.; Berenschot, J. W.; Boer, M. J. D.; Gardeniers, J. G. E.; Jansen, H. V.; Nijdam, W.; Rijn, C. J. M. V.; Elwenspoek, M. C. *IEEE* **2003**, *2*, 1742.
(34) Amandusson, H.; Ekedahl, L. G.; Dannetun, H. *J. Membr. Sci.* **2001**, *193*, 35.
(35) Iyoha, O.; Enick, R.; Killmeyer, R.; Morreale, B. *J. Membr. Sci.* **2007**, *305*, 77.
(36) Morreale, B. D.; Ciocco, M. V.; Howard, B. H.; Killmeyer, R. P.; Cugini, A. V.; Enick, R. M. *J. Membr. Sci.* **2004**, *241*, 219.
(37) McKinley, D. L. U.S. Patent 3439474, 1969.
(38) Polak, M.; Rubinovich, L. *Surf. Sci. Rep* **2000**, *38*, 127.
(39) Abraham, F. F.; Brundle, C. R. *J. Vac. Sci. Technol.* **1981**, *18*, 506.
(40) Hoffmann, M. A.; Wynblatt, P. *Metall. Mater. Trans. A* **1989**, *20*, 215.
(41) Weigand, P.; Novacek, P; Husen, G. v.; Neidhart, T.; Varga, P. *Surf. Sci.* **1992**, *269−270*, 1129.

H

dx.doi.org/10.1021/jp201793d |*J. Phys. Chem. C* XXXX, XXX, 000–000

(42) Wynblatt, P.; Ku, R. C. *Surf. Sci.* **1977**, *65*, 511.

(43) Tsong, T. T.; Ren, D. M.; Ahmad, M. *Phys. Rev. B* **1988**, *38*, 7428.

(44) Mousa, M. S.; Loboda-Cackovic, J.; Block, J. H. *Vacuum* **1995**, *46*, 117.

(45) Newton, M. A.; Francis, S. M.; Li, Y. X.; Law, D.; Bowker, M. *Surf. Sci.* **1991**, *259*, 45.

(46) Bergmans, R. H.; VandeGrift, M.; VanderGon, A. W. D.; Brongersma, H. H. *Surf. Sci.* **1996**, *345*, 303.

(47) Pace, S.; Van Hoof, T.; Hou, M.; Buess-Herman, C.; Reneirs, F. *Surf. Interface Anal.* **2004**, *36*, 1078.

(48) Yuan, L.; Goldbach, A.; Xu, H. *J. Phys. Chem. B* **2007**, *111*, 10952.

(49) Bozzolo, G.; Garces, J. E.; Noebe, R. D.; Abel, P.; Mosca, H. O. *Prog. Surf. Sci.* **2003**, *73*, 79.

(50) Yang, L. *Philos. Mag. A* **2000**, *80*, 1879.

(51) Newton, M. A.; Francis, S. M.; Bowker, M. *Surf. Sci.* **1991**, *259*, 56.

(52) Lovvik, O. M. *Surf. Sci.* **2005**, *583*, 100.

(53) Cheng, Y. C.; Wu, C. J.; Chiang, R. C. *Phys. Rev. B* **1985**, *32*, 4224.

(54) Rousset, J. L.; Bertolini, J. C.; Miegge, P. *Phys. Rev. B* **1996**, *53*, 4947.

(55) Wang, H. Y.; Najafabadi, R.; Srolovitz, D. J. *Interface Sci.* **1993**, *1*, 7.

(56) Prochaska, M.; Jin, J.; Rochefort, D.; Zhuang, L.; Disalvo, F. J.; Abruna, H. D.; Dover, R. B. V. *Rev. Sci. Instrum.* **2006**, *77*.

(57) Xiang, X. D.; Sun, X.; Briceno, G.; Lou, Y.; Wang, K.; Chang, H.; Wolliam, G.; Freedman, W.; Chen, S. W.; Schultz, P. G. *Science* **1995**, *268*, 1738.

(58) Dover, R. B. V.; Schneemeyer, L. F. *Macromol. Rapid Commun.* **2004**, *25*, 150.

(59) Takeuchi, I.; Famodu, O. O.; Read, J. C.; Aronova, M. A.; Chang, K. S.; Craciunescu, C.; Lofland, S. E.; Wuttig, M.; Wellstood, F. C.; Knauss, L.; Orozco, A. *Nat. Mater.* **2003**, *2*, 180.

(60) Hattrick-Simpers, J. R.; Jun, C.; Murakami, M.; Orozco, A.; Knauss, L.; Booth, R. J.; Greve, E. W.; Lofland, S. E.; Wuttig, M.; Takeuchi, I. *Appl. Surf. Sci.* **2007**, *254*, 734.

(61) Park, C.; Bauer, E.; Poppa, H. *Surf. Sci.* **1985**, *154*, 371.

(62) He, J. W.; Jiang, W. L.; Goodman, D. W. *J. Vac. Sci. Technol., A* **1990**, *8*, 2435.

(63) Westerwaal, R. J.; denBesten, C.; Slaman, M.; Dam, B.; Nanu, D. E.; Bottger, A. J.; Haije, W. J. *Int. J. Hydrogen Energy* **2011**, 36.

(64) Cumpson, P. J.; Seah, M. P. *Surf. Interface Anal.* **1997**, *25*, 430.

(65) Hertz, H. *Ann. Phys. (Leipzig)* **1882**, *17*, 177.

(66) Knudsen, M. *Ann. Phys. (Leipzig)* **1915**, *47*, 697.

(67) Rahimi, P.; Ward, C. A. *Int. J. Thermodyn.* **2005**, *8*, 1.

(68) Dean, J. A. *Lange's Handbook of Chemistry*, 15th ed.; Mc-Graw Hill: New York, 1999; Section 6.

(69) Subramaniam, P. R.; Laughlin, D. E. *J. Phase Equilib.* **1991**, *12*, 231.

(70) Skriver, H. L.; Rosengaard, N. M. *Phys. Rev. B* **1992**, *46*, 7157.

(71) Abraham, F. F.; Brundle, C. R. *J. Vac. Sci. Technol.* **1981**, *18*, 506.

(72) Somorjai, G. A. *Introduction to Surface Chemistry and Catalysis*; Wiley: New York, 1994.

(73) Hofmann, S. In *Surface Segregation Phenomena*; CRC Press: Boston, 1990; p 110.

(74) Peacock, D. C. *Appl. Surf. Sci.* **1986**, 27.

(75) Peacock, D. C. *Appl. Surf. Sci.* **1986**, 306.

I

dx.doi.org/10.1021/jp201793d |*J. Phys. Chem. C* XXXX, XXX, 000–000